IEEE Access
Multidisciplinary ⋮ Rapid Review ⋮ Open Access Journal

Received 1 December 2022, accepted 28 December 2022, date of publication 3 January 2023, date of current version 13 January 2023.

Digital Object Identifier 10.1109/ACCESS.2022.3233826

RESEARCH ARTICLE

Study on MPPT Algorithm Based on an Efficient Hybrid Conjugate Gradient Method in a Photovoltaic System

WANG JINPENG[1], YAO QINXUE[1], ZHANG BO[1], JEREMY-GILLBANKS[2], AND ZHAO XIN[1], (Member, IEEE)

[1]School of Information Science and Engineering, Dalian Polytechnic University, Dalian, Liaoning 116039, China
[2]School of Electronic, Electrical and Computer Engineering, The University of Western Australia, Perth, WA 6009, Australia

Corresponding author: Wang Jinpeng (wangjp@dlpu.edu.cn)

This work was supported in part by the Project of the National Natural Science Foundation of China under 61402069, in part by the 2017 and 2020 Projects of the Natural Science Foundation of Liaoning Province under Grant 20170540059 and Grant J2020018, and in part by the General Project of Liaoning Education Department in 2016 under Grant 2016J205.

ABSTRACT An MPPT (Maximum Power Point Tracking) plays a vital role in a photovoltaic(PV) power generation system. Applying the optimum MPPT is a significant way to achieve an efficient PV system. The MPPT methods' efficiency counts on the two MPPT factors, including the perturbation period and the perturbation amplitude. Nevertheless, realizing MPPT in the photovoltaic array is very hard when the natural conditions change, especially for the temperature and light intensity. This paper proposed a new method based on Conjugate Gradient (CG) to address the problem of hard reasonable considering both dynamic and steady-state performance in some existing MPPT algorithms. Meanwhile, the presented algorithm can effectively adjust the output of PV cells by controlling the boost DC/DC converter. Finally, the experimental and simulation results show the system can quickly get the maximum power point and have performance.

INDEX TERMS MPPT, conjugate gradien, photovoltaic system.

I. INTRODUCTION

With the continuous consumption of nonrenewable energy, such as oil, coal, and natural gas, people have paid more and more attention to environmental and energy problems [1], [2], [3]. Solar energy, as specific clean energy, has become prominent. Recently, the research and application of PV generation and its related technologies have made good progress and become one of the hot spots in the new renewable energy research area.

Solar energy is the most significant resource, which means nothing can live without it on earth [4], [5], [6]. Owing to the advancement of technology and the usage of different types of energy, people have determined that the electrical energy produced by applying Solar cells or PV systems is one of the most effective and valuable. Following a research report by the IEA(International Energy Agency), the energy consumption on earth has increased fast in recent years [7], [8], [9].

Due to some advantages, including low noise, minimal depreciation of its components owing to the lack of moving parts, nonpolluting operation after its installation, and lack of cost for the fuel, PV power has been much more popular [10], [11], [12]. The PV energy is simple in design and clean. Also, its best merit is its output from microwatt to megawatt. There are a lot of applications of the PV system, including pumping water [13], power support [14], communications [15], home solar systems [16], power plants [17], and (space vehicles) astronautic applications [18], etc. Because of the widespread usage of this energy, it is ordinary that annual demand is going to increase in this area, also.

Given the physical characteristics of the main building parts of solar cells (semiconductors) and their non-linearity properties, we can find a maximum possible output power

The associate editor coordinating the review of this manuscript and approving it for publication was Giambattista Gruosso.

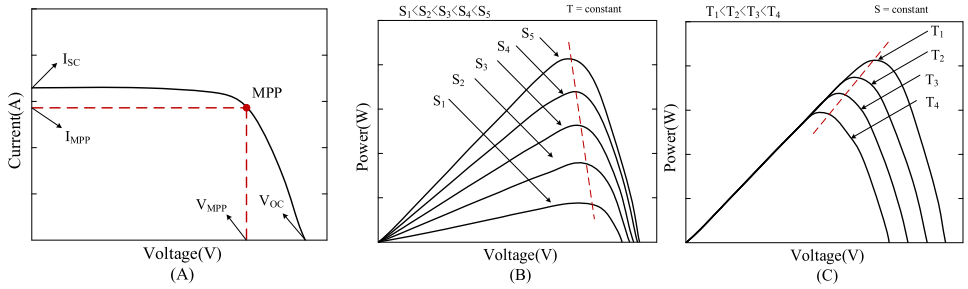

FIGURE 1. Properties of a classic PV cell. a.relation between V_{OC} vs. V_{MPP} and I_{SC} vs. I_{MPP}; b. voltage-power profile under a constant temperature; c. voltage-power profile under unvaried insulation.

from the peak of the power-current (or power-voltage) profile of those solar cells. Commonly, people name this point MPP (Maximum Power Point) [19], [20], [21]. Thanks to some specific characteristics of the building materials of solar cells, MPP changes as a variation of irradiance and temperature shown in figure 1 below. This figure illustrates that the MPP appears near the top of the P–V profile or the famous knee point of the P–V curve. Because the MPP depends on solar radiation (S) and temperature (T), and these environmental conditions vary randomly, the MPP position is continuously changed [22], [23], [24], [25]. Therefore, it is inevitable to apply an MPPT (Maximum Power Point Tracking) technique to keep the working point of a PV system regularly at or at least close to the MPP [26], [28], [29].

Nowadays, there are some availably simple, practical, and feasible MPPT algorithms, including the conductance increment method (INC) [30], the disturbance observation method (P&0) [31], and the constant voltage control way (PV) [32], [33]. In addition, many international researchers gradually would like to introduce the fuzzy PID control method [34], neural network control method [35], fuzzy adaptive control method [36], and automatic intelligent control technique into the field of the PV MPPT [37]. There are three main evaluating indexes for the MPPT methods mentioned above: ① steady-state characteristics, which means the difference between the actual power when reaching the stable working state and the available power under this condition; ② Dynamic factors, which means to find and stabilize the tracking speed of MPP; ③ Implementing cost, which refers to the price of processors and sensors used in a PV MPPT system; Furthermore, some algorithms require additional light and temperature sensors; meanwhile, some methods demand a high-performance processor due to a large amount of computation.

Although there are many MPPT algorithms and comparisons of MPPT methods, most of the literature took aims for only one goal [38], [39]. Overall, it is hard to simultaneously consider the dynamic performance, steady-state performance, and implementation cost of the MPPT [40].

To address the problem mentioned above hard to balance multiple indicators. This paper presents an MPPT algorithm for a photovoltaic system based on the conjugate gradient method. Meanwhile, the tracking process has good steady-state performance and dynamic performance.

Besides part I of the introduction to the background, the rest sections of the paper are as follows: section II presents the system overview; section III discusses the operation principle of an MMPT system; part IV shows the simulation and experiment performed in this paper as well as their analysis; finally, section V concludes the whole article.

II. SYSTEM MODEL

As reviewed above, the PV system needs a specific circuit MPPT to keep the working point always on the MPP or at least near it. Figure 2 below gives the model of an MPPT system. The DC-DC also uses a controller signal and makes the output be the desired level [28]. Therefore, the MPPT algorithms can compute an optimal duty cycle by investigating different parameters (current, temperature, or voltage) and deliver this value to the converter to increase the PV power [29]. Figure 2 below illustrates the model of the MPPT system.

As well known, the MPP system must be in operation ceaselessly in real-time cause the factors on which this system depends (radiation and temperature) always change all day [30], [31], [32]. These changes in the number of temperatures and radiations during the day may be partial shading or perfectly normal [33]. Consequently, it is necessary to rapidly and accurately update the duty cycle (it depends on the circumstances).

A classical PV system comprises an MPPT tracker (power electronic converters and controllers), solar arrays, and load. The efficiency increasing of every part can make improving the PV system. Figure 3 illustrates a practical single diode model of solar cells [34].

Putting those solar cells next one by one can achieve this module. The panel includes connecting some modules, and several selected ones can make up an array further. For instance, linking a parallel or series of modules can create a solar panel. According to the Practical single diode Model of solar cells (as shown in figure 3 above), the VCR (Voltage-Current Relationship) of two terminal circuit networks, and the Kirchhoff theorem in circuits [35], we can define the relationship that is between the current and voltage of the

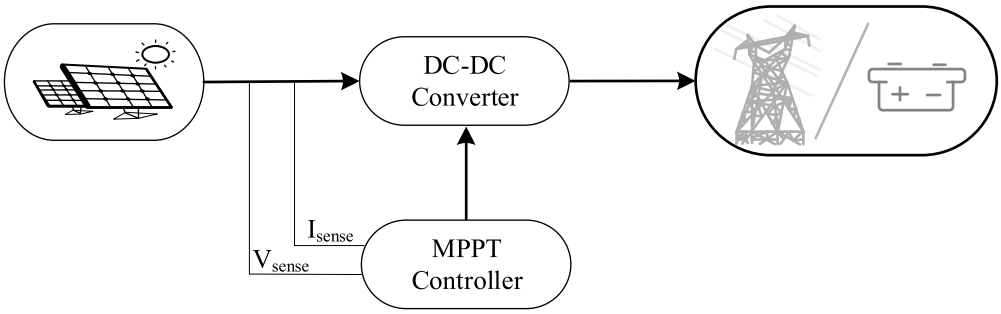

FIGURE 2. The model of the MPPT system.

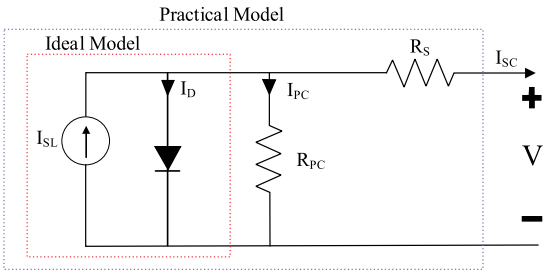

FIGURE 3. Practical single diode model of solar cells.

solar cell as Equation (1) below:

$$I_{SC} = I_{SL} - I_D - I_{PC} = I_{SL} - I_{sr}\left(e^{\frac{q(U_{oc}+I_{sc}R_{SB})}{QKT}} - 1\right) - \frac{U_{oc} + I_{sc}\cdot R_{SB}}{R_{PC}} \quad (1)$$

In Equation (1), I_{sc} means the current of a short circuit, an output current from solar cells; I_{sL} denotes the current achieved directly from the sunlight; I_D symbolizes diode junction current; I_{PC} illustrates the parallel branch circuit current; q shows the charge of an electron; U_{oc} represents the voltage of an open circuit, an output voltage from solar cells. In addition, R_{SB} indicates the resistance of series branch and R_{PC} is the resistance of the parallel circuit; Furthermore, K symbolizes the Boltzmann constant, T shows an absolute temperature of the P–N junction and Q is an ideality factor of a diode;

Last but not least, this paper also lists the other three formulas to explain Equation (1) clearly as below:

$$I_{sr} = I_{srt}\left(\frac{T_{ab}}{T_{ref}}\right)^3 e^{\frac{q}{QK}\left(\frac{1}{T_{ref}} - \frac{1}{T_{ab}}\right)} \quad (2)$$

In expression (2) above, I_{srt} is the saturated reverse current at a reference temperature; T_{ab} symbolizes the absolute temperature of a battery surface; T_{ref} shows the reference temperature.

$$I_{SL} = \frac{\lambda}{100}\left[I_{bsc} + I_{tsc}\left(T_{ab} - T_{ref}\right)\right] \quad (3)$$

In it, I_{bsc} denotes the battery short-circuit current at a reference temperature, and I_{tsc} indicates the temperature coefficient of a short-circuit current.

TABLE 1. Some selected parameters in characteristic equations of solar cells output.

Parameters	Meanings	Units	Values range
q	charge of an electron	C	1.61×10^{-19}
I_{sc}	output current from solar cells	A./Ampere	dynamic
Q	diode quality factor	—	1-5
λ	sunshine intensity coefficient	W/m^2	—
U_{oc}	output voltage from solar cells	V/Volt	dynamic
K	Boltzmann constant	J/K	1.38×10^{-23}
E_G	band gap energy of a battery semiconductor	eV	1-3

$$Q = \frac{\rho}{r} = \frac{\rho}{r_L + r_C} = \frac{\rho}{\frac{\rho}{Q_L} + \rho/Q_C} = \frac{Q_L Q_C}{Q_L + Q_C} \quad (4)$$

Furthermore, we see a parameter Q, a diode quality factor, or a Q factor as a dimensionless parameter in physics and engineering. It is a physical quantity indicating the damping property of the oscillator, and it can also represent the resonance frequency of the oscillator relative to the bandwidth. The high Q factor shows that the rate of energy loss of the oscillator is slow and the vibration can last for a long time.

Table 1 below gives the units and values range of some selected parameters in characteristic equations of Solar cells output:

When calculating the ideal circuit, we can ignore the internal resistances R_s and R_{sh} in solar cells. Consequently, we get a simplified one from the model described via expression (1):

$$I_{SC} = I_{SL} - I_{sr}\left(e^{\frac{qU_{OC}}{QKT}} - 1\right) \quad (5)$$

In practice, PV arrays usually consist of solar cells. When the characteristics of each component of the photovoltaic

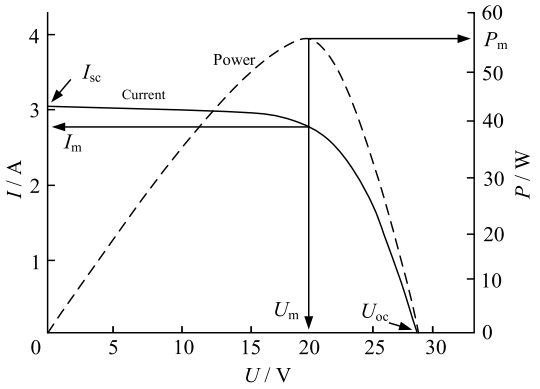

FIGURE 4. The VCR characteristics of PV cells.

array are relatively consistent and the relatively uniform environment, using the above model can obtain the relationship between the output voltage and output current of the photovoltaic array, referred to as VCR characteristics, as shown in Figure 4 below:

III. MPPT IN PV SYSTEM USING HYBRID CONJUGATE GRADIENT METHOD

Due to the classical disturbance observation method and its improved algorithm, the tracking speed and the accuracy of the fuzzy control tracking method are hard to take into account, including two parts: 1. the large the disturbance step is, the faster it is, but the worse the accuracy is; 2. the smaller the step is, the higher the accuracy, but the slower the speed is. Due to continuous disturbance and optimization, the photovoltaic system cannot work stably in the MPP but swings around the MPP, resulting in the loss of power to a certain extent.

This paper sets the MPPT problem as a one-dimensional optimization problem. The proposed method can quickly achieve and stabilize MPP through an iterative algorithm with the optimal step size. The conjugate gradient method can address the above one-dimensional optimization problem and overcome the shortcomings other one-dimensional optimization algorithms have. The rest of this section illustrates the principle and implementation of MPPT in PV systems using the conjugate gradient method.

A. PRINCIPLE OF MPPT IN PV SYSTEMUSING CONJUGATE GRADIENT METHOD

Thinking about a static point problem relevant to an unrestricted nonconvex optimization, find and obtain

$$\boldsymbol{\omega}^* \in \mathbb{R}^d \quad \text{thus to} \quad \nabla f\left(\boldsymbol{\omega}^*\right) = 0. \tag{6}$$

In equation (6) above, $f : \mathbb{R}^d \to \mathbb{R}$ is continuously differentiable. By now, there are some good algorithms for optimizing, just like the Newton method, CG method, the steepest descent method, and quasi-Newton ways. Because the CG methods utilize the CG directions for seeking minimizers of those observed loss functions, thus to address local Nash equilibrium problems both in practice and theory. Therefore, the authors adopt this CG-type algorithm: given $\boldsymbol{\omega}_0 \in \mathbb{R}^d$ and $\boldsymbol{S}_0 := -\nabla f(\boldsymbol{\omega}_0)$, then Z = 98.

$$\boldsymbol{\omega}_{m+1} := \boldsymbol{\omega}_m + \beta_m \boldsymbol{S}_m \tag{7}$$

where,

$$\boldsymbol{S}_{m+1} := -\nabla f\left(\boldsymbol{\omega}_{m+1}\right) + \gamma_{m+1}\boldsymbol{S}_m \tag{8}$$

In expressions (7,8,9) above, $(\beta_m)_{m\in\mathbb{N}}$ represents a sequence of the step sizes (also known as the learning rate in machine learning), operation coefficient $\gamma_{m+1} \in \mathbb{R}_+$, and $\boldsymbol{S}_m$ is CG direction which means the searching direction. The computation of this CG direction $\boldsymbol{S}_{m+1}$ depends not only on the past one $\boldsymbol{S}_m$ but also on its current gradient $\nabla f\left(\boldsymbol{\omega}_{m+1}\right)$.

Because the method uses no inverses operation of matrices, the memory requirement of this algorithm is small. Commonly, there are two main types of CG methods: the linear and nonlinear way.

Here, the authors chose the linear CG algorithm owing to its ability to solve the equations $A\boldsymbol{\omega} = \boldsymbol{b}$ using $\boldsymbol{b} \in \mathbb{R}^d$ and a positive definite matrix A when working in a linear system. That means to minimize $f(\omega) = \frac{\langle \boldsymbol{\omega}, A\boldsymbol{\omega}\rangle}{2} - \langle \boldsymbol{b}, \boldsymbol{\omega}\rangle$ on $\mathbb{R}^d$. When eigenvalues of matrix A comprise d-m smaller eigenvalues, with m large values, the linear algorithm will break at a specific solution only behind $m+1$ steps.

As for the nonlinear type (just like the parameter γ_m), scientists have widely researched it and successfully taken it to practice [36]. These cases illustrate that using the nonlinear type can solve a problem of the large-scale stationary point through a common nonlinear function f. There are some famous parameters γ_m for the nonlinear conjugate algorithm, including HS (Hestenes & Stiefel) [37], DY (Dai& Yuan) [38], PRP (Polak, Ribiere & Polyak) [39], and FR(Fletcher & Reeves) [40]. Their definitions are as the following formulas:

$$\gamma_m^{HS} = \frac{\langle \nabla f\left(\boldsymbol{\omega}_m\right), \nabla f\left(\boldsymbol{\omega}_m\right) - \nabla f\left(\boldsymbol{\omega}_{m-1}\right)\rangle}{\langle \boldsymbol{S}_{m-1}, \nabla f\left(\boldsymbol{\omega}_m\right) - \nabla f\left(\boldsymbol{\omega}_{m-1}\right)\rangle} \tag{9}$$

$$\gamma_m^{DY} = \frac{\|\nabla f\left(\boldsymbol{\omega}_m\right)\|^2}{\langle \boldsymbol{S}_{m-1}, \nabla f\left(\boldsymbol{\omega}_m\right) - \nabla f\left(\boldsymbol{\omega}_{m-1}\right)\rangle} \tag{10}$$

$$\gamma_m^{PRP} = \frac{\langle \nabla f\left(\boldsymbol{\omega}_m\right), \nabla f\left(\boldsymbol{\omega}_m\right) - \nabla f\left(\boldsymbol{\omega}_{m-1}\right)\rangle}{\|\nabla f\left(\boldsymbol{\omega}_{m-1}\right)\|^2} \tag{11}$$

$$\gamma_m^{FR} = \frac{\|\nabla f\left(\boldsymbol{\omega}_m\right)\|^2}{\|\nabla f\left(\boldsymbol{\omega}_{m-1}\right)\|^2} \tag{12}$$

In addition, a WH (W. W. & Hager) index is from a specific modification of the HS equation as below:

$$\gamma_m^{WH} = \gamma_m^{HS} - \mu \times \frac{\left[\nabla f\left(\boldsymbol{\omega}_m\right) - \nabla f\left(\boldsymbol{\omega}_{m-1}\right)\right]^3 \langle \nabla f\left(\boldsymbol{\omega}_m\right), S_{m-1}\rangle}{\langle S_{m-1}, \nabla f\left(\boldsymbol{\omega}_m\right) - \nabla f\left(\boldsymbol{\omega}_{m-1}\right)\rangle^2} \tag{13}$$

In equation (13) above, $\mu > 1/4$.

Furthermore, other researchers [52], [53], [54] would like to adopt the hybrid conjugate gradient methods, such as:

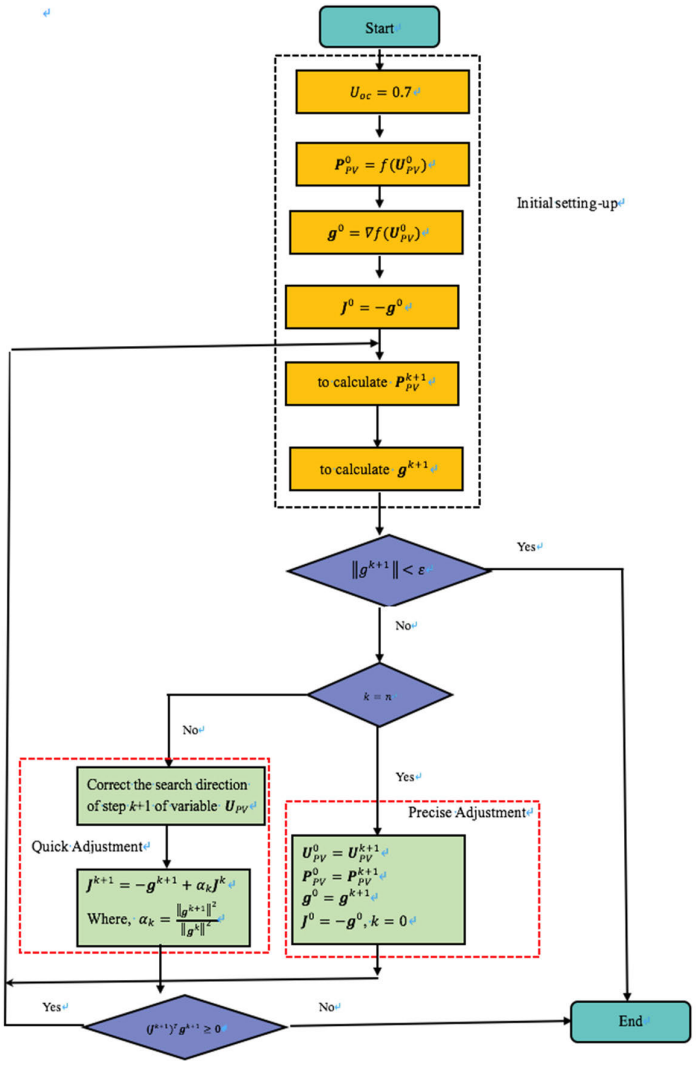

FIGURE 5. Flowchart for MPPT algorithm.

combining the FR and PRP methods and a combination of the HS and DY methods:

$$\gamma_m^{FR-PRP} = max\left\{0, min\left\{\gamma_m^{FR}, \gamma_m^{PRP}\right\}\right\} \quad (14)$$

$$\gamma_m^{HS-DY} = max\left\{0, min\left\{\gamma_m^{HS}, \gamma_m^{DY}\right\}\right\} \quad (15)$$

As seen in formulas (14,15) above, the hybrid methods are selective ways or switch ones. And this paper used the former algorithm of combining the FR and PRP methods due to its low complexity and easy implementation.

B. ALGORITHM IMPLEMENTATION OF MPPT IN PV SYSTEM USING CONJUGATE GRADIENT METHOD

For the MPPT algorithm, it is a one-dimensional optimization of the maximum value with U_{PV} as the independent variable and P_{PV} as the function. According to the solar cell model formula (5), figure 5 below shows the definition and the flowchart of this presented algorithm:

As shown in figure 5, there are three types of modules: firstly, the 1st type has three Condition judgment modules noted via a diamond with blue; in addition, the 2nd type has nine operational process boxes, and the former six boxes with yellow mean the initial setting-up; also, the rest three boxes with green are the model for quick adjustment, and the model for precise adjustment respectively.

To illustrate the method more clearly, table 3 below lists the steps of the algorithm further:

Because it can not directly solve the first order differential of the U-P curve in figure 4, the paper adopts a numerical calculation method. Moreover, this article utilized an algorithm of the simplest difference quotient approximate derivative (i.e., $\frac{dP_{PV}}{dU_{PV}} \approx \frac{P_k - P_{k-1}}{U_k - U_{k-1}}$) to decrease the computational complexity. Therefore, from the specific iterative algorithm, using the current three consecutive working points can calculate the voltage value of the next time. Then, repeating this cycle can approach the MPP step by step.

TABLE 2. The LFSR in the work mode.

Algorithm 1. The LFSR in the work mode

{Begin

$S_{16} = \{2^{15}S_{15} + 2^{17}S_{13} + 2^{21}S_{10} + 2^{20}S_4$

$+ (1 + 2^8)S_0\}$

$mod(2^{31} - 1)$;//Generate S_{16}.

If $S_{16} = 0$ then

set $S_{16} = 2^{31} - 1$; //

Initialization again.

else

$(S_1, S_2, \cdots, S_{15}, S_{16}) \rightarrow (S_0, S_1, \cdots, S_{14}, S_{15})$

Endif;

End;}

NOTE Please:All denotations "//" of the tables in this paper mean an explanation of the program before it.

TABLE 3. The steps of MPPT of photovoltaic system using conjugate gradient method.

Algorithm 2. MPPT of photovoltaic system using conjugate gradient method

1 To reduce the number of iterations, the initial iteration value is initially 0.7 times the open circuit voltage U_{oc};

2 Meanwhile, $\boldsymbol{P}_{PV}^0 = f(\boldsymbol{U}_{PV}^0)$, $\boldsymbol{g}^0 = \nabla f(\boldsymbol{U}_{PV}^0)$, and$\boldsymbol{J}^0 = -\boldsymbol{g}^0$.

3 Carry out a one-dimensional search according to

4 formula (7), and calculate$\boldsymbol{P}_{PV}^{k+1}$, $\boldsymbol{g}^{k+1}$..

5 Terminate the iteration once meeting its termination

6 condition of$\|\boldsymbol{g}^{k+1}\| < \varepsilon$, or operate step (4).

When $k = n$, the iteration has no endpoint, you must reset the initial point, thus to $\boldsymbol{U}_{PV}^0 = \boldsymbol{U}_{PV}^{k+1}$,

7 $\boldsymbol{P}_{PV}^0 = \boldsymbol{P}_{PV}^{k+1}$, $\boldsymbol{g}^0 = \boldsymbol{g}^{k+1}$, $\boldsymbol{J}^0 = -\boldsymbol{g}^0$;

8 *and* $k = 0$. *Jump to step (2), or proceed to (5).*

9 Correct the search direction of step k+1 of variable $\boldsymbol{U}_{PV}$, $\boldsymbol{J}^{k+1} = -\boldsymbol{g}^{k+1} + \alpha_k \boldsymbol{J}^k$, and jump to step (2), where $\alpha_k = \frac{\|\boldsymbol{g}^{k+1}\|^2}{\|\boldsymbol{g}^k\|^2}$.

If $(\boldsymbol{J}^{k+1})^T \boldsymbol{g}^{k+1} \geq 0$occurs (i.e., the algorithm fails), then reset the initial point, and jump to step (2).

IV. SIMULATION RESULTS AND EXPERIMENTAL RESULTS AND THEIR ANALYSIS

A. SIMULATION RESULTS AND ANALYSIS

According to the system model, the authors established a simulation model of the PV array with the MPPT function

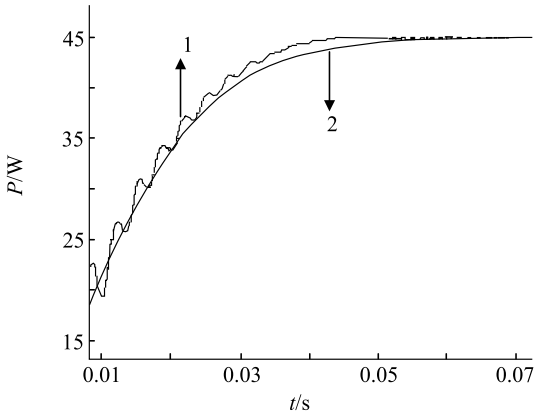

(a). the dynamic state working process response.

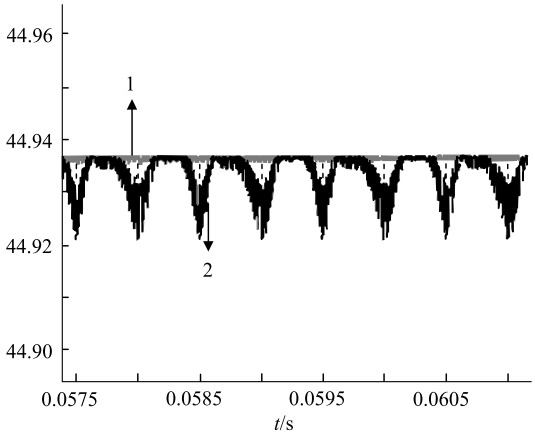

(b). the Steady state working process response.

FIGURE 6. Output power response.

in Matlab / Simulink environment. The simulation utilized the Backward Differentiation Formulas of ode23tb (stiff-TR-BDF) in MATLAB, and the initial conditions are as follows: illumination 1 kW / m^2, environment temperature 25 °C. The simulation in this article is under an ideal situation without partial shading.

Figure 6 above compares the output power between the fuzzy control tracking method and the proposed hybrid conjugate gradient method. Curves 1 and 2 in the figure are the tracking profiles obtained by the fuzziness control method and the proposed hybrid conjugate gradient one, respectively. As shown in figure 6(a), the proposed hybrid conjugate gradient method has a smaller dynamic and is easy to meet the steady state (shown in figure 6(b)). That means the proposed algorithm has better performance.

Figure. 7 shows the dynamic process of the proposed conjugate gradient method when the light intensity and temperature change: the light intensity changes from 0.8kw/m^2 to 1 kW / m^2, and the temperature changes from 0 ° C to 25 ° C. Although there is a power pulse at about P = 35W and t = 0.5s, the proposed algorithm tracked the MPP soon in

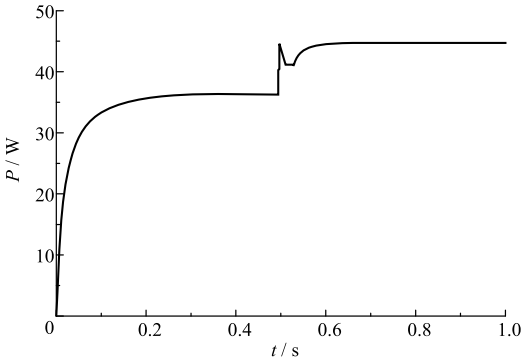

FIGURE 7. The MPPT curve when the temperature and light intensity all change.

0.05 seconds. That means that the proposed algorithm works well.

B. EXPERIMENTAL RESULTS AND ANALYSIS

To test the effectiveness of the proposed algorithm. This article not only carried out a Matlab/Simulink simulation of the control system but also experiments with the hardware circuit based on a classic DSP chip of TMS320F2812 as the core control. Figure 8 below gives the implementation of a block diagram of the MPPT system hardware structure.

From figure 8 above, the experimental hardware platform is a solar power supply system with a power of 200W. The core circuit connects to the power supply and the load through the boost circuit. The main switch tube adopts IGBT, and the load circuit includes a battery and adjustable resistance. The control circuit concludes with an interface circuit, drive circuit, and core control circuit with a DSP chip of TMS320F2812 as the key controller. TMS320F2812 has a high frequency of 150 MHz, fast command operation speed, multi-channel PWM, and 12-bit a A/D conversion, which can best improve the data processing ability and control accuracy of the control system. The interface circuit mainly involves Hall voltage and current sensors with high accuracy. RLC design principles require sufficiently low resistance RDS (ON) and relatively low grid charge, and its switching frequency is about 300 kHz.

Figure 9 above shows the experimental platform for DSP implementation, and the components shown in this figure correspond to figure 8 before. Figure 10 above gives some experimental hardware, including an oscilloscope, D/A converter, and a chip of the TMS320F2812 used in DSP implementation.

Figure 11 below shows the experimental results. The weather was clear, and the sunshine was uniform during the experiment. To quickly approach the MPP, first set an initial voltage of the solar panel to be 0.7 times of the open circuit

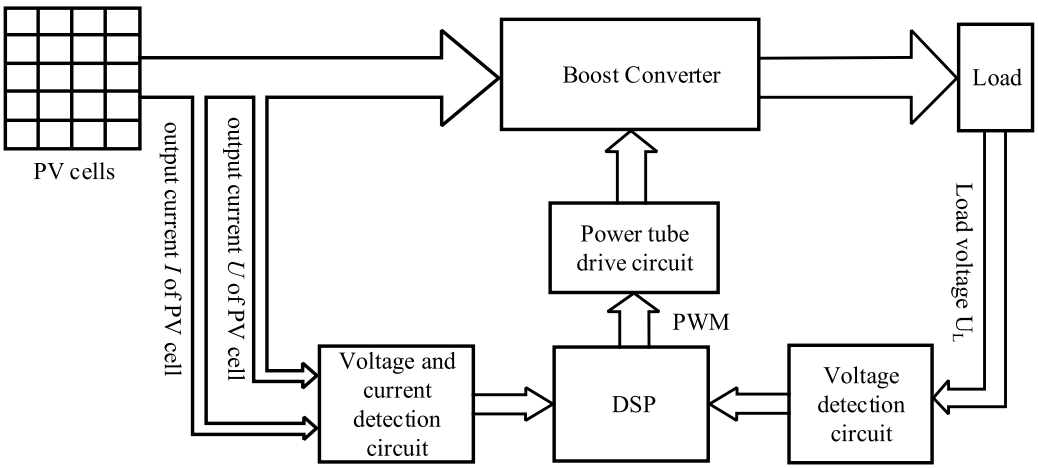

FIGURE 8. Structure block diagram of photovoltaic MPPT system.

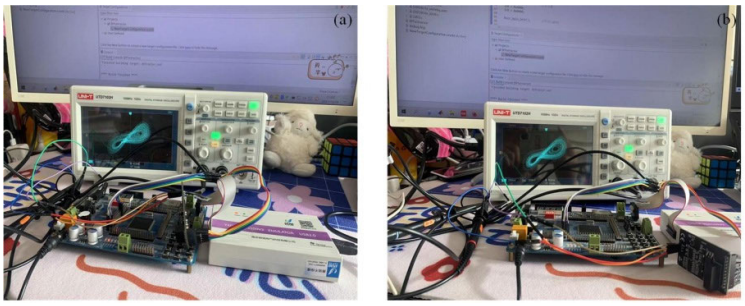

FIGURE 9. Experimental platform for DSP implementation.

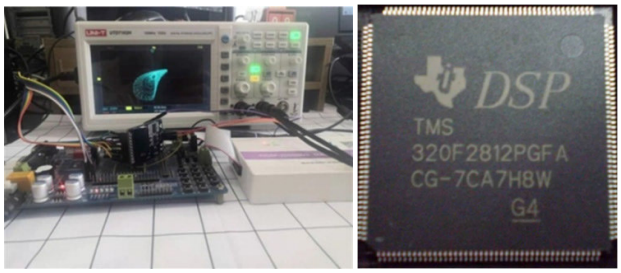

FIGURE 10. The isolated components for the hardware implementation.

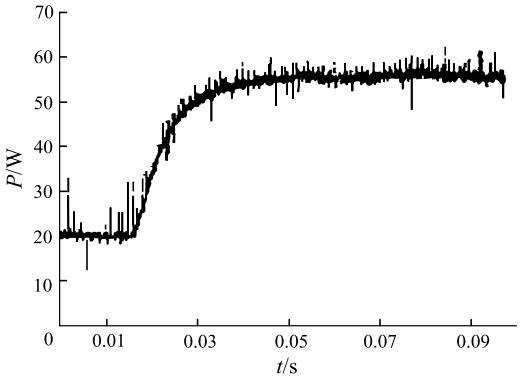

FIGURE 11. The MPPT curve when the temperature and light intensity all change.

TABLE 4. Comparisons to the traditional methods.

Dataset	Scheme	SGD	M-SGD	Proposed CG
MNIST	Constant	67.95	51.02	41.34
CIFAR	Constant	132.76	193.92	116.68

and then start the presented MPPT algorithm. This figure denotes that the MPP is in 25 $\sim$ 30ms approximately.

The loss function is non-convex as well as high-dimensional in our experimental setup. So, an easy gradient norm does not necessarily conform to the quality of learning for the Generative Adversarial Networks (GANs). This paper assessed the training on the real-world data by using a metric of FID (Fréchet inception distance) usually applied for evaluating the quality of learning for GANs. This paper utilized the statistical information achieved by transforming the fake and real images using a neural network to measure the FID. The less the metric value is, much better the training for the generator of GANs has. Table 4 below gives Comparisons to the traditional methods.

Table 4 compares the FID marks of the training model by the other methods and the proposed CG way. It depicts that the presented CG method is better than the traditional algorithm (momentum SGD and the SGD) in terms of the schedule with a constant learning rate.

V. CONCLUSION

An optimum MPPT method is vital to achieving an efficient PV system. Usually, the efficiency of an MPPT algorithm is up to two MPPT factors the perturbation period and the perturbation amplitude. This optimization of the MPPT methods can decide both the steady-state oscillation and the tracking speed. To address the problem of how to balance the dynamic and steady-state performance in an MPPT system. This paper proposes an Efficient hybrid conjugate gradient algorithm mixed FR and PRP ways in a photovoltaic system to obtain the MPPT as the natural characters of the light intensity and temperature change. Both the simulation and experimental results prove the presented algorithm works well.

AUTHOR CONTRIBUTIONS

Wang Jinpeng: Designed the measurement scheme, carried out the simulations, and wrote the article; Yao Qinxue, Zhang Bo, and Jeremy-Gillbanks: Performed the field test and analyzed the data; and Zhao Xin: Supervised the work, arranged the architecture, and contributed to the writing of the article.

CONFLICTS OF INTEREST

The authors declare no conflict of interest.

REFERENCES

[1] *Internationalization of Domestic Cryptographic Algorithm Standards Creates New Achievements ZUC Algorithm Officially Becomes the ISO/IEC International Standard*. [Online]. Available: http://www.oscca.gov.cn/sca/xwdt/202005/11/content_1060747.shtml.2020

[2] N. Drucker and S. Gueron, "Fast constant time implementations of ZUC-256 on ×86 CPUs," in *Proc. 16th IEEE Annu. Consum. Commun. Netw. Conf. (CCNC)*, Jan. 2019, pp. 1–7, doi: 10.1109/CCNC.2019.8651851.

[3] W. Jinpeng, Y. Zhengpeng, J. Gillbanks, T. M. Sanders, and Z. Nianyu, "A novel linear antenna synthesis for linear dispersion codes based on an innovative HYBRID Genetic algorithm," *Symmetry*, vol. 11, no. 9, p. 1176, 2019.

[4] D. Zhang, A. Zhao, X. Yang, Y. Sun, and J. Xiao, "Generalized synchronization between Chen system and Rucklidge system," *IEEE Access*, vol. 7, pp. 8519–8526, 2019.

[5] X. Liu, X. Bi, H. Yan, and J. Mou, "A chaotic oscillator based on meminductor, memcapacitor, and memristor," *Complexity*, vol. 2021, pp. 1–16, Dec. 2021.

[6] T. Liu, H. Yan, S. Banerjee, and J. Mou, "A fractional-order chaotic system with hidden attractor and self-excited attractor and its DSP implementation," *Chaos, Solitons Fractals*, vol. 145, Apr. 2021, Art. no. 110791.

[7] T. Liu, S. Banerjee, H. Yan, and J. Mou, "Dynamical analysis of the improper fractional-order 2D-SCLMM and its DSP implementation," *Eur. Phys. J. Plus*, vol. 136, no. 5, p. 506, May 2021.

[8] C. Ma, J. Mou, P. Li, and T. Liu, "Dynamic analysis of a new two-dimensional map in three forms: Integer-order, fractional-order and improper fractional-order," *Eur. Phys. J. Special Topics*, vol. 230, nos. 7–8, pp. 1945–1957, Aug. 2021.

[9] X. Li, J. Mou, Y. Cao, and S. Banerjee, "An optical image encryption algorithm based on a fractional-order laser hyperchaotic system," *Int. J. Bifurcation Chaos*, vol. 32, no. 3, Mar. 2022, Art. no. 2250035.

[10] X. Gao, J. Mou, L. Xiong, Y. Sha, H. Yan, and Y. Cao, "A fast and efficient multiple images encryption based on single-channel encryption and chaotic system," *Nonlinear Dyn.*, vol. 108, no. 1, pp. 613–636, Mar. 2022, doi: 10.1007/s11071-021-07192-7.

[11] X. Gao, J. Mou, S. Banerjee, Y. Cao, L. Xiong, and X. Chen, "An effective multiple-image encryption algorithm based on 3D cube and hyperchaotic map," *J. King Saud Univ. Comput. Inf. Sci.*, vol. 34, no. 4, pp. 1535–1551, Apr. 2022, doi: 10.1016/j.jksuci.2022.01.017.

[12] X. Ma, J. Mou, J. Liu, C. Ma, F. Yang, and X. Zhao, "A novel simple chaotic circuit based on memristor–memcapacitor," *Nonlinear Dyn.*, vol. 100, no. 3, pp. 2859–2876, 2020.
[13] R. Tang, J. Duan, and H. Deng, "Image encryption algorithm based on Logistic chaotic sequels and DES," (in Chinese), *J. Comput. Appl.*, vol. 3, no. 5, pp. 89–92, 2017.
[14] J. S. Sousa and J. P. Vilela, "A characterization of uncoordinated frequency hopping for wireless secrecy," in *Proc. 7th IFIP Wireless Mobile Netw. Conf. (WMNC)*, Vila Moura, Portugal, May 2014, pp. 1–4.
[15] A. Boonkajay and F. Adachi, "PAPR reduction for STBC transmit diversity with transmit FDE using blind selected mapping," Presented at the IEEE VTS Asia Pacific Wireless Commun. Symp. (AP-WCS), Incheon, South Korea, Aug. 2017.
[16] D. Sun, Q. Zhang, D. Wei, and M. Zhang, "A secure constellation design for polarized modulation in wireless communications," *IEEE Access*, vol. 8, pp. 130589–130597, 2020.
[17] W. Chao, L. Pengcheng, and L. Rui, "Security frequency hopping communication system based on an improved ZUC algorithm," (in Chinese), *Tsinghua Univ., Sci. Technol.*, vol. 59, no. 2, pp. 154–161, 2019.
[18] X. T. Feng, "The ZUC stream cipher algorithm," (in Chinese), *J. Inf. Secur. Res.*, vol. 2, no. 11, pp. 1028–1041, 2016.
[19] J. K. M. S. U. Zaman and R. Ghosh, "Review on fifteen statistical tests proposed by NIST," *J. Theor. Phys. Cryptogr.*, vol. 1, pp. 18–31, Nov. 2012.
[20] X. Wang and H.-L. Zhang, "A novel image encryption algorithm based on genetic recombination and hyper-chaotic systems," *Nonlinear Dyn.*, vol. 83, nos. 1–2, pp. 333–346, 2016.
[21] A. N. Bikos and N. Sklavos, "Architecture design of an area efficient high speed crypto processor for 4G LTE," *IEEE Trans. Depend. Sec. Comput.*, vol. 15, no. 5, pp. 729–741, Sep. 2018, doi: 10.1109/TDSC.2016.2620437.
[22] X. Jin, Y. Chen, S. Ge, K. Zhang, X. Li, Y. Li, Y. Liu, K. Guo, Y. Tian, G. Zhao, X. Zhang, and Z. Wang, "Color image encryption in CIE L*a*b*: Space," in *Proc. 6th Int. Conf. Appl. Techn. Inf. Secur. (ATIS)*. Berlin, Germany: Springer-Verlag, 2015, pp. 74–85.
[23] L. Xu, Z. Li, J. Li, and W. Hua, "A novel bit-level image encryption algorithm based on chaotic maps," *Opt. Lasers Eng.*, vol. 78, no. 21, pp. 17–25, Mar. 2012.
[24] Design Team, "ZUC-256 stream cipher," *J. Cryptol. Res.*, vol. 5, no. 2, pp. 167–179, 2018, doi: 10.13868/j.cnki.jcr.000228.
[25] W. Jinpeng, C. Fan, and Z. Nianyu, "Multi carrier system joint receiving method based on MAI and ICI," *J. Jilindaxue*, vol. 41, no. 6, pp. 1793–1797, 2018.
[26] J. Wang, Y. Zhengpeng, J. Gillbanks, T. M. Sanders, and N. Zou, "A power control algorithm based on chicken game theory in multi-hop networks," *Symmetry*, vol. 11, no. 5, p. 718, May 2019.
[27] J. G. Andrews, S. Buzzi, C. Wan, S. V. Hanly, A. Lozano, A. C. K. Soong, and J. C. Zhang, "What will 5G be?" *IEEE J. Sel. Areas Commun.*, vol. 32, no. 6, pp. 1065–1082, Jun. 2014.
[28] Y. Niu, Y. Li, D. Jin, L. Su, and A. V. Vasilakos, "A survey of millimeter wave communications (mmWave) for 5G: Opportunities and challenges," *Wireless Netw.*, vol. 21, no. 8, pp. 2657–2676, Nov. 2015.
[29] E. Turgut and M. C. Gursoy, "Average error probability analysis in mmWave cellular networks," in *Proc. IEEE IEEE Veh. Technol. Conf. (VTC-Fall)*, Boston, MA, USA, Sep. 2015, pp. 1–5.
[30] *Study on Supporting 256-Bit Algorithms for 5G*, document TR33.841, 3GPP, 2018.
[31] Design Team, "ZUC-256 stream cipher," *J. Cryptol. Res.*, vol. 5, no. 2, pp. 167–179, 2018, doi: 10.13868/J.cnki.jcr.000228.
[32] P. Ekdahl, T. Johansson, A. Maximov, and J. Yang, "A new SNOW stream cipher called SNOW-V," IACR Cryptol. ePrint Arch., Lyon, France, Tech. Rep. 2018/1143, 2018. [Online]. Available: http://eprint.iacr.org//2018/1143.pdf
[33] G. Han and J. Song, "Extensions of the I-MMSE relationship to Gaussian channels with feedback and memory," *IEEE Trans. Inf. Theory*, vol. 62, no. 10, pp. 5422–5445, Oct. 2016.
[34] J. Zhang, S. Zhang, and J. Wang, "Pseudorange measurement method based on AIS signals," *Sensors*, vol. 17, no. 5, p. 1183, May 2017.
[35] K. Zheng, Q. Hu, and J. Zhang, "Positioning error analysis of ranging-mode using AIS signals in China," *J. Sensors*, vol. 2016, Aug. 2016, Art. no. 6928961.
[36] M. Hu, Y. Li, X. Lu, and H. Zhang, "Tone reservation to minimize nonlinearity impact on OFDM signals," *IEEE Trans. Veh. Technol.*, vol. 64, no. 9, pp. 4310–4314, Sep. 2015.
[37] B. Mondal, T. Thomas, E. Visotsky, F. Vook, A. Ghosh, Y.-H. Nam, Y. Li, J. Zhang, M. Zhang, Q. Luo, Y. Kakishima, and K. Kitao, "3D channel model in 3GPP," *IEEE Commun. Mag.*, vol. 53, no. 3, pp. 16–23, Mar. 2015.
[38] R. Guido and D. Conforti, "A hybrid genetic approach for solving an integrated multi-objective operating room planning and scheduling problem," *Comput. Oper. Res.*, vol. 87, pp. 270–282, Nov. 2017.
[39] W. Jinpeng, C. Fan, and Z. Nianyu, "Cooperative distributed antenna transmission method based on co-channel interference in 5G mobile communication system," *J. Jilindaxue*, vol. 48, no. 1, pp. 333–341, 2020.
[40] J. Barrueco, J. Montalban, E. Iradier, and P. Angueira, "Constellation design for future communication systems: A comprehensive survey," *IEEE Access*, vol. 9, pp. 89778–89797, 2021.
[41] Z. Babar, Z. B. K. Egilmez, L. Xiang, D. Chandra, R. G. Maunder, S. X. Ng, and L. Hanzo, "Polar codes and their quantum-domain counterparts," *IEEE Commun. Surveys Tuts.*, vol. 22, no. 1, pp. 123–155, 1st Quart., 2020.

WANG JINPENG was born in Wulanhaote, Xingan, China, in 1979. He received the B.S. and M.S. degrees in electronic engineering from the Dalian University of Technology, Dalian. His current research interest includes numerical optimization.

YAO QINXUE received the B.S. and M.S. degrees in electronic engineering from the University of Tju, Tianjin, in 2020. She is currently pursuing the postgraduate degree with the School of Information Science and Engineering, Dalian Polytechnic University, Dalian, Liaoning, China.

ZHANG BO received the B.S. degree in electronic engineering from the University of Haerbin Technology, Heilongjiang, China, in 2001. He is currently pursuing the postgraduate degree with the School of Information Science and Engineering, Dalian Polytechnic University, Dalian, Liaoning, China.

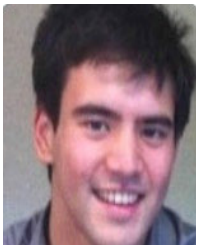

JEREMY-GILLBANKS was born in Perth, WA, Australia, in 1977. He received the B.S. and M.S. degrees in electronic engineering from The University of Western Australia, Australia, in 2016, where he is currently pursuing the Ph.D. degree with the School of Electronic, Electrical and Computer Engineering. He has authored and coauthored several research articles indexed in either Scopus or Web of Science.

ZHAO XIN (Member, IEEE) was born in Jinzhou, Liaoning, China, in 1968. He received the B.S. and M.S. degrees from Jilin University, Changchun, in 1996. He is currently a Professor with Dalian Polytechnic University, Dalian, Liaoning. His current research interest includes numerical optimization.